

Acousto-optic-tunable-filter-based spectropolarimetric imagers for medical diagnostic applications— instrument design point of view

Neelam Gupta

Army Research Laboratory
2800 Powder Mill Road
Adelphi, Maryland 20783-1197
E-mail: ngupta@arl.army.mil

Abstract. Compact optical imagers that can detect both spectral and polarization signatures are required in many biomedical applications. An acousto-optic-tunable-filter (AOTF)-based imager is ideally suited to provide both agile spectral and polarization signatures. Such an imager can be readily used for real-time *in vivo* medical diagnostic applications. We develop a family of small, robust, and programmable hyperspectral imagers operating from the ultraviolet (UV) to the long-wave IR (LWIR). Such imagers require minimal data processing because they can acquire images at only select wavelengths of interest. We use AOTFs made of KDP, TeO₂, and TAS with Si-based CCD, InGaAs, InSb, and HgCdTe cameras to cover different spectral regions from the UV to the LWIR. Operation of each of these imagers and image acquisition is computer controlled. The most developed imager covers the visible to near-infrared (VNIR) region from 400 to 900 nm, with a 10-nm spectral resolution at 600 nm, it uses an electronically tunable TeO₂ AOTF as a bandpass filter, and a nematic liquid crystal retarder to change polarization. We describe our concept in the development of these imagers and present new results obtained using the VNIR imager. © 2005 Society of Photo-Optical Instrumentation Engineers. [DOI: 10.1117/1.2102507]

Keywords: spectropolarimetric; acousto-optic tunable filter; hyperspectral; polarization; imager.

Paper SS04252R received Dec. 17, 2004; revised manuscript received Jul. 6, 2005; accepted for publication Jul. 6, 2005; published online Oct. 14, 2005.

1 Introduction

Biomedical applications require the development of novel instruments that can use optical imaging for medical diagnostics.¹⁻³ Better detection and recognition can be done using both spectral and polarization signatures from the object. Spectral features arise due to the material properties of objects, as a result of the emission, reflection, and absorption of light. The polarization features arise from the physical nature of the object surfaces and edges that influence the polarization properties of the reflected, transmitted, scattered, or emitted light. Using a hyperspectral imager, one can acquire images with narrow spectral bands and take advantage of the characteristic spectral signatures of different materials that make up objects and backgrounds. By combining both polarization and hyperspectral detection capabilities in one single imager, we can perform much better object detection and identification than by using just the polarization or hyperspectral capability. Such imagers can be easily used for real-time *in vivo* medical imaging applications. Traditional hyperspectral imaging systems use gratings and prisms and acquire images in hundreds of bands, requiring a huge amount of data processing. In general, object detection requires spectral im-

ages at a few bands that change based on the object and background scenarios. This clearly establishes a need to design adaptive imaging systems.

An imager designed using an acousto-optic tunable filter (AOTF) is ideally suited to provide both agile spectral and polarization signatures. At the U.S. Army Research Laboratory (ARL), we are developing small, vibration-insensitive, robust, remotely controlled, and programmable hyperspectral imagers covering the ultraviolet (UV) to the long-wave IR (LWIR) spectral regions. Such imagers require minimal data processing because they can collect data at only select wavelengths of interest and the selected wavelengths can be changed based on the scenes of interest. The time to change wavelengths is very fast (in tens of microseconds). This agility in data collection is quite critical for hyperspectral applications because it greatly reduces the data processing requirements associated with the vast quantity of data collection and utilization normally required with traditional hyperspectral imaging systems. A noncollinear AOTF is also a polarization-sensitive device because the two diffracted beams from it are orthogonally polarized. There are two possible imager architectures that are used for a spectropolarimetric imager—in the first, two separate cameras are used with the two diffracted beams to obtain images with orthogonal polarizations, and in

Address all correspondence to Neelam Gupta, AMSRD-ARL-SE-EE, U.S. Army Research Laboratory, 2800 Powder Mill Road, Adelphi, MD 20783-1197. Tel.: (301) 394-2451; Fax: (301) 394-5270; E-mail: ngupta@arl.army.mil

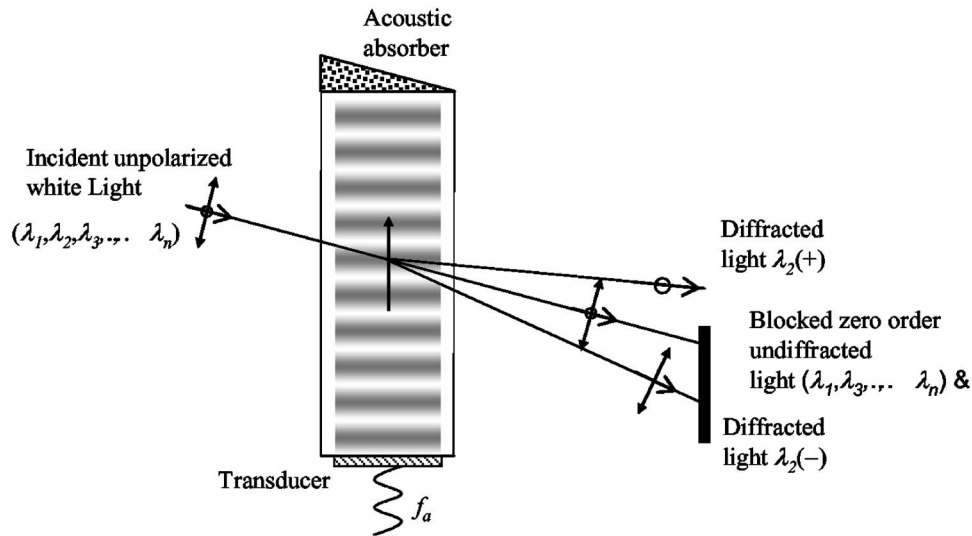


Fig. 1 Filtering operation of a noncollinear AOTF.

the second, only one diffracted beam is imaged with a single camera and a spectrally tunable retarder is used to change the polarization of the incident light to obtain images at orthogonal polarizations.

A number of different noncollinear AOTFs fabricated in different birefringent crystals with different cameras are used to cover the wavelengths from UV to LWIR. We use a KDP AOTF with an extended range response Si charge-coupled device (CCD) camera to cover the UV to visible region⁴ from 220 to 480 nm. A TeO₂ AOTF with an off-the-shelf Si CCD camera covers the visible to near-IR (VNIR) region⁵ from 400 to 900 nm. A TeO₂ AOTF covers the short-wave IR (SWIR) region from 900 to 1700 nm with a room temperature InGaAs camera.⁶ Another TeO₂ AOTF with a liquid-nitrogen-cooled InSb camera covers the midwave IR (MWIR) region^{6,7} from 2 to 4.5 μm . Finally, a TAS (thallium arsenic selenide) AOTF with a liquid-nitrogen-cooled HgCdTe camera covers the LWIR region from 7.8 to 10.3 μm . Each imager has a suitable optical train.^{6,7} In our imager design, only one of the diffracted beams from the AOTF is used with a spectrally tunable nematic liquid crystal variable retarder (LCVR). Such a retarder is placed in the optical train before the AOTF and two retardance values corresponding to the horizontal and vertical incident polarization are used for each spectral band.⁵ The LCVR can be used to cover wavelength regions from 400 nm to 4.5 μm . The operation of each imager and its image acquisition is computer controlled. The TeO₂ AOTF-based VNIR imager with a commercially available electronically tunable LCVR is the most developed im-

ager. It has a 10-nm spectral resolution at 600 nm. Each spectral image is acquired with two retardation values corresponding to the horizontal and vertical incident polarization of light.^{5,8,9} Here we describe the basic concept behind the design of these imagers and the imager development at ARL, and present new imaging results with the VNIR imager.

2 Spectropolarimetric Imager Basics

To understand the wavelength tuning operation of such imagers, it is important to know how a noncollinear AOTF works. In an AOTF, a radio frequency (rf) signal is applied to a piezoelectric transducer that is attached to a birefringent crystal to produce an ultrasonic wave that travels through the crystal. This sets up a moving diffraction grating in the crystal. The sound wave is absorbed by an acoustic absorber on the opposite crystal facet after it traverses the crystal. When unpolarized white light is incident on such a crystal, it is diffracted by the traveling acoustic wave, producing two diffracted beams with orthogonal polarizations—one with a Doppler upshifted and the other with a Doppler downshifted optical frequency for a given applied rf—based on the phase-matching condition. (The Doppler shift is negligible for the optical frequencies.) In our imager design we use only one of the two diffracted beams and block the other diffracted beam as well as the undiffracted beam, as shown in Fig. 1. The diffracted optical wavelength can be tuned by changing the applied rf. The tuning relationship and the spectral resolution for a noncollinear filter, using wide-angle diffraction geom-

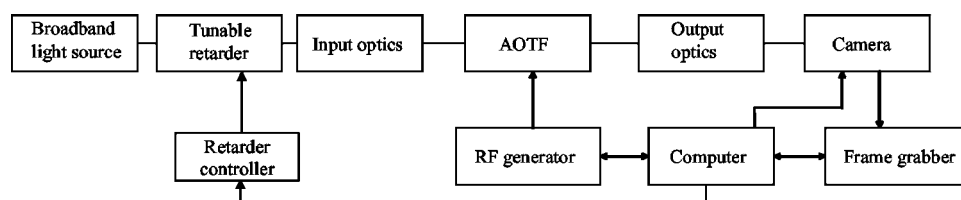


Fig. 2 Block diagram of a spectropolarimetric imaging system.

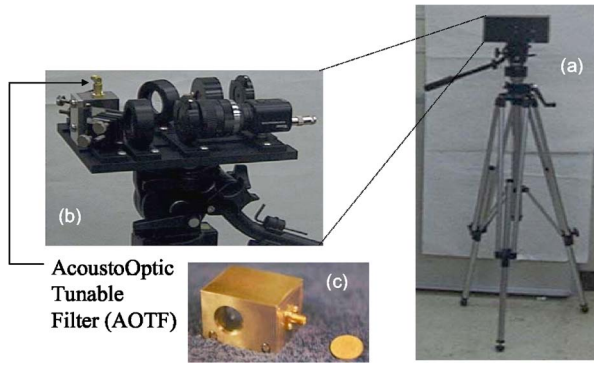


Fig. 3 VNIR spectropolarimetric imager: (a) imager box mounted on a tripod, (b) optical breadboard, and (c) photograph of AOTF cell.

etry, can be approximated by the following equations:^{10,11}

$$\lambda_0 = \frac{\Delta n V}{f_a} (\sin^2 2\theta_i + \sin^4 \theta_i)^{1/2}, \quad (1)$$

and

$$\frac{\Delta\lambda}{\lambda_0} = \frac{0.9\lambda_0}{L\Delta n \sin^2 \theta_i} \equiv \frac{1}{R}, \quad (2)$$

where λ_0 is the diffracted optical wavelength, Δn is the birefringence of the material (difference of two refractive indices), V is the acoustic velocity in the material, f_a is the applied rf signal (same as the acoustic frequency), θ_i is the optical angle of incidence with respect to the crystal optic axis, L is the length of AO interaction in the crystal (same as the length of the transducer), $\Delta\lambda$ is the optical passband, and R is the spectral resolution. It is clear from Eq. (1) that the optical wavelength can be changed by changing applied rf because λ_0 increases as f_a decreases or vice versa.

To obtain polarization information, we placed a spectrally tunable LCVR in front of the AOTF, and two retardance values corresponding to the horizontal and vertical polarizations for each wavelength are used. The tuning of such a retarder is done by changing the applied voltage. The retardance values used are 0 and 90 deg, corresponding to net incident horizon-

tal and vertical polarizations, respectively. The diffracted beam from the AOTF is imaged on a CCD camera.⁵ By tuning the filtered wavelength over the entire tuning range, we can acquire a hyperspectral image cube corresponding to each polarization.^{5,9} Since both the retarder and the AOTF are tuned electronically, no moving parts are involved, and our imager is adaptive and robust as compared to other traditional hyperspectral imagers. The block diagram of an AOTF spectropolarimetric imager's operational layout is shown in Fig. 2.

3 Imager Development

As discussed earlier, at ARL we have developed a family of AOTF-based spectropolarimetric/hyperspectral imagers covering wavelength regions from the UV to the LWIR using AOTFs fabricated in different birefringent acousto-optic (AO) materials in combination with appropriate camera and optics.⁴⁻⁷ Our filter designs are based on the consideration that for a spectral imaging instrument we need a fairly broad bandpass and a large linear as well as angular aperture such that there is a substantial light throughput. In our program, we are developing new AOTF cells and materials for fabricating such cells and we have developed both KDP and MgF_2 cells operating from vacuum UV to visible wavelengths. For the LWIR, we have developed an AOTF cell in TAS and are now growing Hg_2Br_2 crystals to fabricate AOTFs operating in the range from 0.4 to 30 μm . We have also developed cells operating over greater than one octave range in wavelength. We have used these imagers to carry out a variety of experiments in object detection.⁵⁻⁹ The UV imager has been used to investigate vegetation samples on quartz microscope slides.⁴ Recently, performance of this imager was further improved by the development of a new AOTF with a larger angular field of view. All of the imagers are used to carry out transmission, reflection, and absorption measurements, while both the UV and the VNIR imagers can be used for fluorescence measurements as well.^{1,3}

As mentioned earlier, the VNIR imager is the most developed system among all our imagers. Now, we focus on this imager. The noncollinear TeO_2 AOTF used in this imager was fabricated with a 10-nm bandpass at 600 nm with an input aperture of $1.5 \times 1.5 \text{ cm}^2$, and an angular aperture of 4.2 deg.

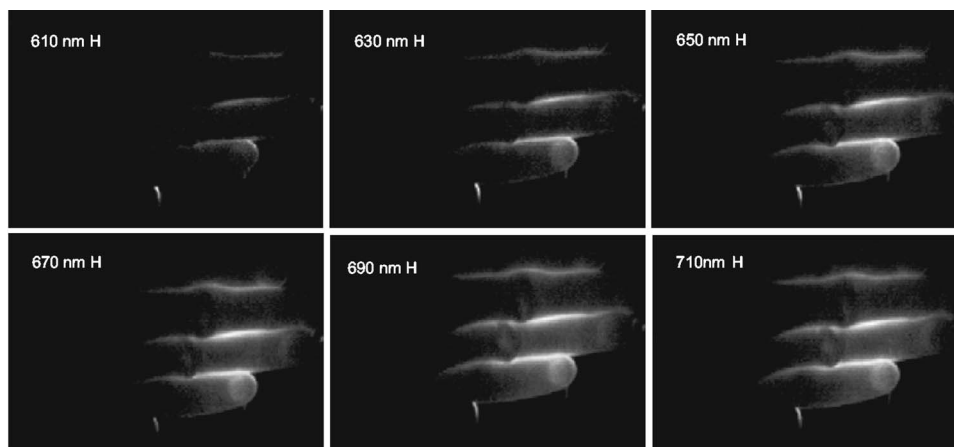


Fig. 4 Spectral images of a human hand with horizontal polarization.

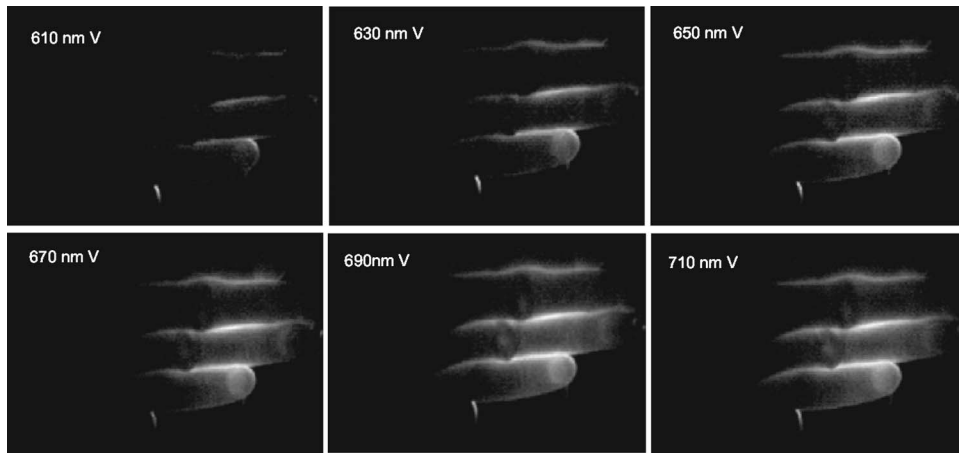


Fig. 5 Spectral images of a human hand with vertical polarization.

A thin-plate $1.5 \times 0.5 \text{ cm}^2$ LiNbO_3 transducer was bonded on it using cold indium vacuum welding. Both the electrical and acoustic impedance matching were done carefully to couple most of the applied rf power into the crystal as acoustic power. A wedge was used on the output facet of the AOTF to eliminate the spectral scene shift of the output diffracted beam. The filter is operated with a horizontally polarized incident beam that results in a vertically polarized diffracted beam. The filter operates in the rf range from 60 to 120 MHz, corresponding to the wavelength range from 400 to 880 nm. The diffraction efficiency of the filter is close to 95% with 0.9 W of rf power. The acoustic velocity in this crystal is 650 m/s, and for a 1.5-cm aperture we can change the frequency every 23 μs . Based on this, in theory we can obtain 4.33×10^4 spectral image frames per second. The size of the VNIR imager is $20 \times 15 \times 10 \text{ cm}^3$ and it weighs⁵ less than 2 kg.

4 Experiment

Our long-term motivation is using this imager for a medical diagnostics. As a preliminary experiment to check our system's capabilities, we chose to image a human hand with our imager to see what results we get. We carried out a transmis-

sion experiment to obtain spectropolarimetric images using our VNIR imager, as shown in Fig. 3. We recorded spectropolarimetric images of a fair-skinned Caucasian hand placed in front of a white light source using the light transmitted through the hand. The hand was placed in such a way that no light leaked through between fingers. Images were recorded from 400 to 800 nm with a 10-nm spectral interval. The wavelength was changed by varying the applied rf between 50 and 120 MHz to correspond to the desired optical wavelength range. The rf power used was less than 1.0 W. Each spectral image was recorded with two orthogonal polarizations of light. Both the rf synthesizer and the LCVR were controlled using a personal computer. The CCD output was captured and digitized using a frame grabber and stored on the computer hard drive. The size of each stored image was 640×480 pixels. The operation of the imager was seamless with a graphical user interface.

5 Results and Analysis

Some examples of the spectropolarimetric images obtained with our imager in the experiment are presented here. As mentioned earlier, in this experiment we collected transmission images of a human hand in front of a white light source.

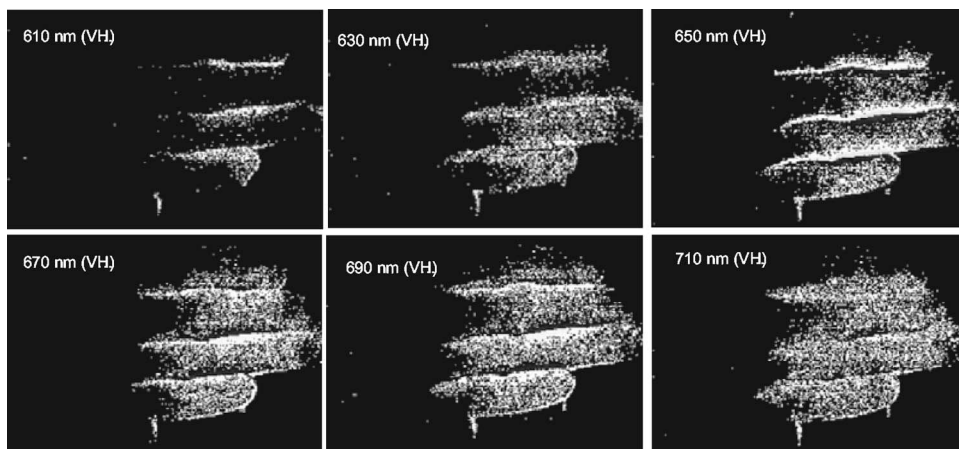


Fig. 6 Polarization difference images of a human hand at six wavelengths.

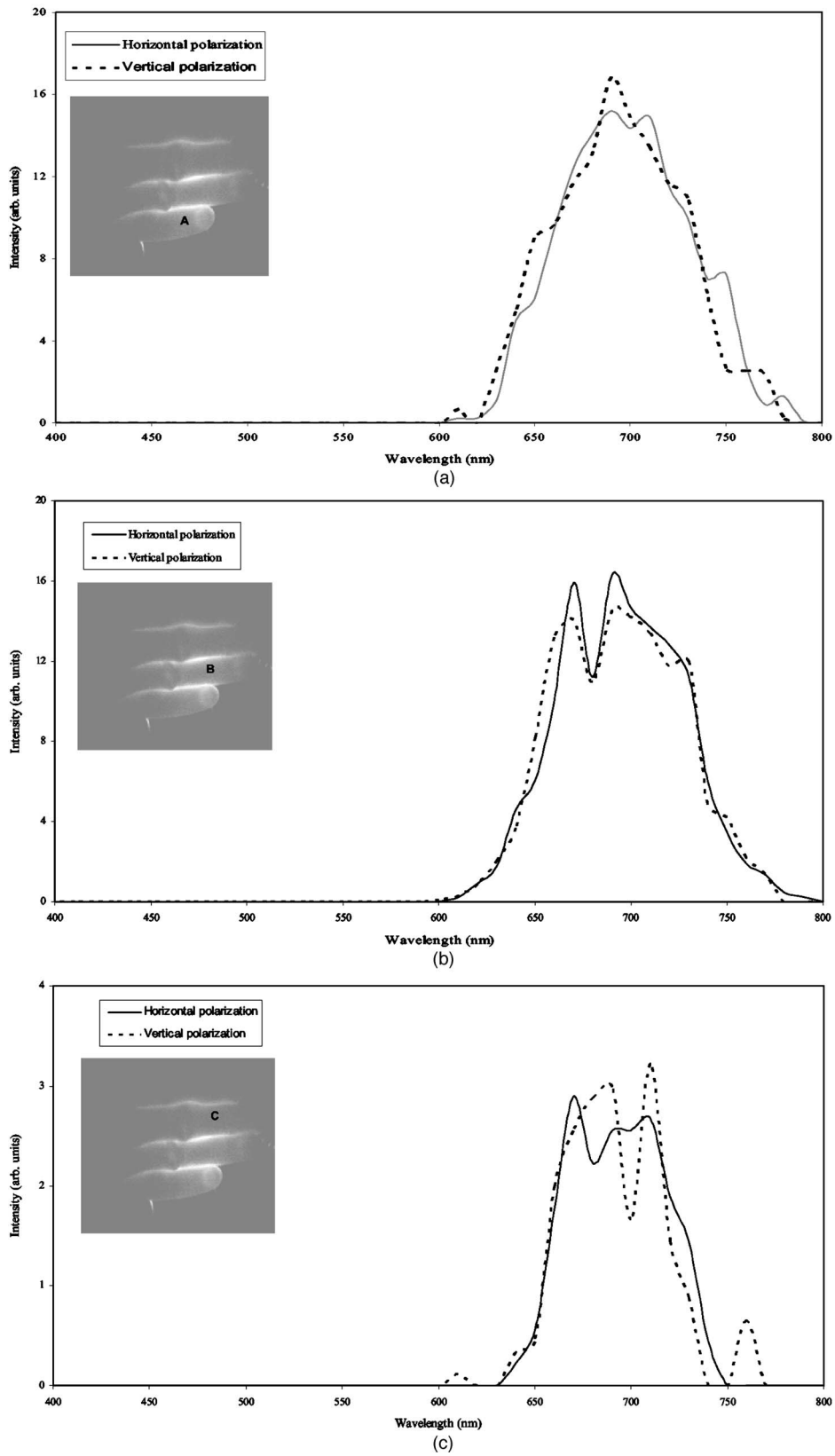


Fig. 7 Spectra of points (a) A, (b) B, and (c) C, respectively (shown on image inset) for the two polarizations.

The spectral images were collected at 41 spectral bands from 400 to 800 nm at 10-nm interval. At each spectral band, images were acquired with two retardation values corresponding to the horizontal and vertical polarizations of the light incident on the imager. Figures 4 and 5 show spectral transmission image of a human hand collected with the horizontal and the vertical polarizations, respectively at six sample wavelengths—610, 630, 650, 670, 690, and 710 nm. Figure 6 shows the corresponding polarization difference (vertical–horizontal) images.

The images at 41 bands were used to construct a hyper-spectral image cube for each polarization of light transmitted by the hand using commercial hyperspectral image processing software ENVI 4.1. (RSI, Boulder, Colorado). Two such image cubes were constructed—one for the horizontal and the other for the vertical polarization. The size of each image cube is 12.6 Mbytes. These image cubes can be used to obtain spectral plots corresponding to any point on the 640×480 size spatial image. The spectra of three points marked on the images as A, B, C are shown in Figs. 7(a)–7(c), respectively, for the two polarizations. These points were randomly selected on the three fingers to show the corresponding spectra. Intensity value at each point was obtained by averaging over a 3×3 pixel square. Also, to obtain spectra, the two image cubes were linked such that there was an exact pixel-by-pixel correspondence for every spectral image in the image cube. (In other words, each spectral frame in the horizontal polarization image cube was coregistered with the corresponding spectral frame in the vertical polarization image cube in the software.) Note that even though the human hand imaged was roughly 1 in. thick, it transmitted much light between 600 and 800 nm due to scattering in the tissue, while no light was transmitted from 400 to 600 nm due to absorption as expected.¹² In the single polarization images, light intensity is greater near the sides of the fingers where the two fingers are held together. The images at the two polarizations in Figs. 4 and 5 look fairly alike to a human observer but the polarization difference images in Fig. 6 clearly show significant spectral and polarization signatures for various features in the images. The polarization signatures for various fingers change as a function of wavelength, the index finger not visible in either of the pure polarization images starts showing up in the polarization difference images at wavelengths of 650 nm and higher. Also it is easy to make out the nails and skin folds at the knuckles in these rather low intensity images. It is apparent from the intensity distribution in Figs. 7(a)–7(c) that the spectra corresponding to the three points exhibit some polarization dependence even though there is no consistent pattern for the three points chosen. The intensity at points A and B are close but it is a factor of 5 lower at C.

6 Summary and Conclusions

We developed a family of compact, portable, agile spectropolarimetric imagers using an AOTF as the light dispersive element in combination with a camera appropriate for the spectral range of operation. A commercially available LCVR was used for polarization selection with VNIR and SWIR imagers.

The VNIR imager is the most developed system in our suite of imagers. This imager was used from 400 to 800 nm with a 10-nm interval to acquire spectral images at 41 bands with retardance settings of 0 and 90 deg at each wavelength corresponding to horizontal and vertical polarization of the transmitted light from a human hand. The spectral analysis was performed using a commercial software package ENVI 4.1. This analysis clearly showed that a human hand, even though roughly 1 in. thick, transmits a fair amount of light from 600 to 800 nm, while no light is transmitted between 400 and 600 nm, and there is a noticeable difference in the images obtained at two orthogonal polarization of the transmitted light based on the polarization difference images. The parts of the hand not visible in the images with either horizontal or vertical polarization show up in the polarization difference images. The drop-off in the intensity at longer wavelengths is mainly due to the drop in the sensitivity of our imager. Further work must be done to understand the source of the polarization features in these images and how it can be utilized for medical diagnostics (i.e., differences between tumors and surrounding healthy tissues). We also plan to use our other imagers for similar investigations.

Based on our results, note that AOTF-based imagers offer useful capabilities for data acquisition for noninvasive *in vivo* medical imaging applications in either hyperspectral or spectropolarimetric modes because such imagers are compact and agile with no moving parts and have an automated operation.

References

1. G. C. Tang, J. T. Chen, A. Katz, E. J. Celmer, R. W. Krumm, and R. R. Alfano, "Ultraviolet-visible acousto-optic tunable spectroscopic imager for medical diagnosis," *J. Biomed. Opt.* **3**, 80–84 (1998).
2. "Investigating the body with light," *Opt. Photonics News* **15**, 8 (2004).
3. T. Vo-Dinh, D. L. Stokes, M. B. Wabuyele, M. E. Martin, J. M. Song, R. Jagannathan, E. Michaud, R. J. Lee, and X. Pan, "A hyperspectral imager for *in vivo* optical diagnostics," *IEEE Eng. Med. Biol. Mag.* 40–49 (Sept.–Oct. 2004).
4. N. Gupta and V. Voloshinov, "Hyperspectral imager from ultraviolet to visible using KDP AOTF," *Appl. Opt.* **43**, 2752–2759 (2004).
5. N. Gupta, R. Dahmani, and S. Choy, "Acousto-optic tunable filter based visible-to near-infrared spectropolarimetric imager," *Opt. Eng.* **41**, 1033–1038 (2002).
6. N. Gupta, R. Dahmani, K. Bennett, S. Simizu, D. R. Suhre, and N. B. Singh, "Progress in AOTF hyperspectral imagers," in *Automated Geo-Spatial Image and Data Exploitation*, W. E. Roper and M. K. Hamilton, Eds., *Proc. SPIE* **4054**, 30–38 (2000).
7. N. Gupta and R. Dahmani, "Tunable infrared hyperspectral imagers," in *Proc. Int. Symp. on Spectral Sensing Research (ISSSR)*, pp. 233–236 (2001).
8. N. Gupta, "Remote sensing using hyperspectral and polarization images," in *Instrumentation for Air Pollution Global Atmospheric Monitoring*, J. O. Jensen and R. L. Spellicy, Eds., *Proc. SPIE* **4574**, 184–192 (2001).
9. N. Gupta, L. Denes, M. Gottlieb, D. Suhre, B. Kaminsky, and P. Metes, "Object detection using a field-portable spectropolarimetric imager," *Appl. Opt.* **40**, 6626–6632 (2001).
10. N. Gupta, "Acousto-optic tunable filters," *Opt. Photonics News* **8**, 23–27 (1997).
11. M. S. Gottlieb, "Acousto-optic tunable filters," Chap. 4 in *Design and Fabrication of Acousto-Optic Devices*, A. Goutzoulis and D. Pape, Eds., pp. 197–283, Marcel Dekker, New York (1994).
12. R. R. Anderson and J. A. Parrish, "The optics of human skin," *J. Invest. Dermatol.* **77**, 13–19 (1981).